TANDEM-BLADE CENTRIFUGAL COMPRESSOR DESIGN AND OPTIMIZATION BY MEANS OF 3D INVERSE DESIGN

Ricardo Oliveira,
Advanced design Technology, 30 Millbank, Westminster, London SW1P 4DU, UK,
r.oliveira@adtechnology.com
Luying Zhang
Advanced design Technology, 30 Millbank, Westminster, London SW1P 4DU, UK,
l.zhang@adtechnology.com
Mehrdad Zangeneh
Department of Mechanical Engineering, University College London, Torrington Place, London WC1E 7JE, UK, m.zangeneh@ucl.ac.uk

ABSTRACT

In centrifugal compressor design, previous studies have shown the potential of achieving enhanced performance through the inclusion of tandem blades. The conventional design method for this type of machines is based in splitting a baseline impeller into main and tandem blade, and applying appropriate pitch-wise and streamwise displacements. This simple design method has been proven insufficient in achieving better performance than the baseline design, without extra design modifications.

In this paper, a design workflow based in a 3D inverse design method is specifically assembled and applied to the tandem-blade design of centrifugal compressors. The blade geometry is controlled by imposing specified distributions of blade loading in tandem and main blades. Starting from an initial full blade design, different tandem-blade designs are generated using the inverse design methodology. Performance of the initial and optimized designs are then assessed by 3D CFD analysis at design and off-design conditions. The mechanism of performance improvement is investigated in detail. In addition, the structural performance of the generated designs is also assessed by means of FEA.

KEYWORDS

tandem-blade compressor, inverse design method, optimization

NOMENCLATURE

$\dot{m}$	mass flow rate	$\boldsymbol{\lambda}$	circumferential clocking fraction
R	radius	$\boldsymbol{\Delta}$	variation
$\boldsymbol{r\overline{V_\theta}}$	circumferential averaged circulation	EXD	exducer
$\boldsymbol{r\overline{V_\theta^*}}$	normalized $\boldsymbol{r\overline{V_\theta}}$	IND	inducer
$\boldsymbol{\partial r\overline{V_\theta^*}/\partial m}$	streamwise blade loading	LE	leading edge
V	velocity	HUB	hub
P	pressure	SHR	shroud
$\boldsymbol{\alpha}$	pitch angle	IN	inlet
$\boldsymbol{\theta}$	circumferential direction	OUT	outlet
$\boldsymbol{\gamma}$	wrap angle	DYN	dynamic
$\boldsymbol{\eta}$	efficiency		

INTRODUCTION

In this paper, a design/optimization methodology of centrifugal compressor with tandem blade configuration is presented. The tandem impeller configuration refers to the division of an impeller in two separate blades: inducer and exducer. There are mainly three benefits compared to a full blade impeller design: First, providing some extent of pressure rise, the inducer presence allows for an alleviation of the workload on the radial exducer blade. This can have benefits on operating range, efficiency and exit flow uniformity. Second, this configuration can be seen as a flow control method, where the close proximity of inducer trailing edge (TE) and exducer leading edge (LE) generates a jet effect that can prove beneficial to the exducer flow separation control. Lastly, the interruption of the boundary layer growth can possibly improve efficiency and flow uniformity.

Previously, various researchers have attempted to use the tandem configuration to obtain improved performance against a known design. First publications date back to an experimental campaign by Klassen et al. [1]. After this, various authors have published studies, some of them with contradicting conclusions. Bache [2] performed a numerical parametric study on a centrifugal compressor, reporting gains in discharge flow uniformity, and concluding that clocking fraction was the primary driver for the improvements seen. Roberts and Kacker [3] also found, from numerical studies, a high influence of clocking fraction in pressure ratio and efficiency, also obtaining improved outlet flow uniformity. Ju and Zhang [4] show one of the few studies where an optimization approach is taken to the design of tandem impellers, performing experimental studies on an optimized design and also identifying a more uniform discharge flow, although with lower efficiency.

Josuhn-Kadner and Hoffmann [5] and Josuhn-Kadner [6] investigated, experimentally and numerically, a centrifugal compressor with varying inducer positions, obtaining an increased stable operating range with the tandem configuration. Danish et al. [7] has attempted a redesign of a turbocharger centrifugal compressor without changes to the camber distribution, concluding that the tandem-blade design only showed improvements at near choke flow. Erdmenger and Michelassi [8] also reported that the tandem configuration can yield significant improvements at off-design conditions, while only slight improvements were seen at design point. Shi et al. [9] studied numerically how the tandem configuration can improve centrifugal pump performance, reporting that the pump performance at low flow rates was considerably improved. Li et al. in [10] and [11] reported, with numerical studies exploring inducer/exducer matching characteristics, an improved operating range by 16.7% when using the tandem impeller configuration. Recently, Cuturi et al. [12] were able to redesign a turbocharger compressor by using a tandem radial compressor, designing it by varying the circumferential displacement and axial gap between inducer and exducer blades, achieving higher pressure ratio and improved stall and choke margin.

Danish et al. [13] presented an experimental and numerical study, where, for a design with reduced inducer thickness, a 0.5% efficiency improvement was achieved. Li et al. [14] also presented an interesting numerical investigation on the topic, where improved performance is obtained for a final tandem design, mostly by the performance improvement of downstream components. This design required an adjustment in blade angle and thickness distribution.

Most of the previous works presented have been based in a straightforward cut of existing designs, lacking a design methodology that actively takes into account the coupling between inducer and exducer. These studies show that the design of tandem compressor should be performed in a holistic manner, carefully addressing the coupling effect between inducer and exducer, and not simply performing blade cut of an existing full blade design. To address this issue, in the current work, the 3D inverse design solver TURBOdesign1 [15] is used for the generation of blade shapes. The method, introduced by Zangeneh [16], uses an iterative process to compute blade shape and 3D inviscid flow field. The circumferentially averaged circulation $r\overline{V_\theta}$, normalized by the impeller outlet tip radius and speed ($r\overline{V_\theta^*}$), is specified at LE and TE, determining the work produced. Streamwise blade loading,

defined as the meridional derivative of $r\overline{V_\theta^*}$ is then defined and used to shape the blade geometry by directly controlling the flow field. The details of the 3D inverse design methodology can be found in [16]. This method is particularly advantageous in tandem blade design as the work split between the inducer and exducer can be directly controlled through the specification of $r\overline{V_\theta^*}$, rather than an iterative process based on blade angle adjustment. The method can be used for 3D geometry generation of inducer and exducer blades without numerous design iterations.

Previous application of the 3D inverse design solver has been performed on centrifugal compressors with both full blade and splitter configurations [17]. This work extends the application of 3D inverse design method to tandem blade design. A full workflow is assembled around the 3D inverse design solver TURBOdesign1 (TD1), allowing for the generation of exducer and inducer blades by specifying the work load split and the circumferential shift between blades. The stacking of the blade can be controlled through the specified wrap angle distribution at the TE in TD1. The remaining wrap angle distribution for the exducer blade is computed by the inverse design solver. The inducer wrap angle spanwise distribution at the TE can then be obtained by adding the circumferential shift to the exducer wrap angles at LE, available from the TD1 solution. With this approach, the inverse design solver can generate the matching exducer and inducer blades in a fully connected workflow.

Furthermore, a detailed understanding of the loss generation mechanisms in this type of compressors is not yet available in literature. Zhang et al. [18], have proposed a loss analysis methodology based on quantifying entropy generation through decomposing the flow domain into different regions based on the different loss mechanism. The methodology has been applied to centrifugal [18] and axial compressor [19]. The same analysis is now applied to the tandem blade designs and the results are compared against the initial full blade design. The loss analysis provides new insights into the loss mechanisms that benefit performance in relation to full blade designs.

The single stage compressor specification from Ziegler et al. [20] is used to demonstrate the design methodology. The compressor is firstly used to assemble and validate the computational fluid dynamics (CFD) model to be used. Through CFD and structural finite element analysis (FEA), the efficiency, pressure ratio, stall and choke margins and structural stresses of the Radiver design are obtained. A mesh sensitivity study has been carried out. Two different mesh levels have been chosen - one used for design iterations and the other for entropy analysis as it requires a finer mesh level to resolve the entropy generation near wall [18]. A tandem-blade compressor design is firstly obtained through 3D inverse design method as a baseline design. A design of experiments (DOE) is then performed, varying 3 parameters specific of the tandem-blade configuration, with the main goal of increasing efficiency. From the DOE, an optimized design is achieved and used to compare against the initial Radiver design.

TANDEM-BLADE DESIGN METHODOLOGY

The main challenges specific to tandem-blade compressor design relate to a few design parameters. First, the loading extent of each blade needs to be decided (which will be varied in the optimization phase). The inducer provides some pressure rise, in this way reducing the required loading on the exducer blade. Understanding to which extent the inducer loading improves performance is imperative. The work split, $r\overline{V_\theta^*}_{ratio}$, which is defined as

$$r\overline{V_\theta^*}_{ratio} = \frac{r\overline{V_\theta^*}_{EXD,TE} - r\overline{V_\theta^*}_{EXD,LE}}{r\overline{V_\theta^*}_{IND,TE} - r\overline{V_\theta^*}_{IND,LE}} \quad (1)$$

Second, the circumferential positioning of the inducer blade, relative to the exducer will control the jet effect on the exducer suction surface. The circumferential clocking fraction, λ, is defined as

$$\lambda = \frac{\gamma_{EXD,LE} - \gamma_{IND,TE}}{\alpha_{pitch}} \quad (2)$$

With α_{pitch} being the pitch sector angle, $\alpha_{pitch} = \frac{360°}{N_{blades}} = 24°$. The circumferential clocking fraction $\boldsymbol{\lambda}$ is specified as a spanwise distribution from hub to shroud. Figure 1 illustrates the definition of the circumferential clocking fraction with a blade-to-blade view of a compressor with tandem-blade arrangement.

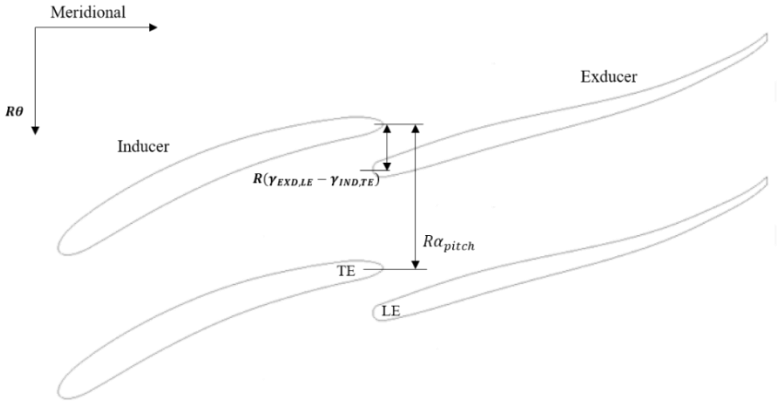

Figure 1 – Illustration of circumferential clocking fraction with blade to blade view of tandem compressor.

The wrap angles at the exducer leading edge, $\gamma_{EXD,LE}$, and at inducer trailing edge, $\gamma_{IND,TE}$, are spanwise distributions, computed as follows: 1) $\gamma_{EXD,TE}$ distribution is a TD1 input. The remaining of the blade wrap angles are determined by the inverse design solver, making $\gamma_{EXD,LE}$ an output from TD1 when solving for the exducer blade. 2) $\gamma_{IND,TE}$ is then computed using Equation (2), by specifying a spanwise λ distribution: $\gamma_{IND,TE} = \gamma_{EXD,LE} - \lambda * \alpha_{pitch}$.

For the baseline design, $\lambda_{Baseline}$ is initially determined. At the hub, inducer LE is placed 9.4º away from the exducer LE ($\lambda_{Baseline,HUB} = 39.19\%$). This value of hub circumferential clocking allows sufficient distance between blades for the generation of fillets for the structural model. At the shroud, the inducer TE is placed 5.7º away from the exducer LE ($\lambda_{Baseline,SHR} = 23.77\%$). The full spanwise distribution is presented in Figure 2.

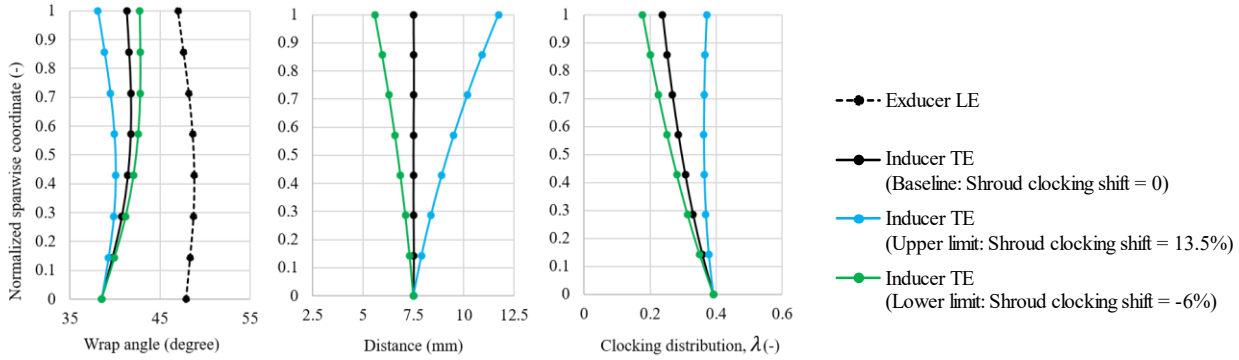

Figure 2 - Exducer LE and Inducer TE matching; Wrap angle, distance and clocking spanwise distributions for baseline design and upper and lower limits of shroud clocking shift used during DOE.

During optimization, to compute the circumferential clocking distribution for a new design, $\lambda_{new\ design}$, a linear shift, $\Delta\lambda$, is applied to the baseline circumferential clocking distribution: $\lambda_{new\ design} = \lambda_{Baseline} + \Delta\lambda$. The linear spanwise shift is defined as $\Delta\lambda = \Delta\lambda_{HUB} + Span_{norm} * \Delta\lambda_{SHR}$. As λ_{HUB} is kept constant, $\Delta\lambda_{HUB} = 0$, and $\Delta\lambda_{SHR}$ is used as design variable.

As seen in Figure 2, a value of $\Delta\lambda_{SHR}$ different than zero leads to a linearly shifted clocking distribution in relation to the baseline design ($\Delta\lambda_{SHR,Baseline} = 0$). The shroud clocking shift value $\Delta\lambda_{SHR}$ is a design variable, which will be varied during the optimization. $\Delta\lambda_{SHR}$ is varied between -6% and 13.5%, distributions represented in Figure 2 (green and blue curves, respectively).

Finally, the meridional extent of inducer and exducer blades, and consequently, the meridional overlapping, are the final parameters to take into account. These parameters are defined for the baseline tandem design and are fixed during the optimization procedure.

During the optimization procedure, the wrap angle spanwise distribution of the exducer blade at the trailing edge, $\gamma_{EXD,TE}$ will also be varied, as this is also an input for the inverse design solver. This specification will not interfere with the workflow detailed for the tandem blade arrangement. $\gamma_{EXD,TE}$ is linearly varied from hub to shroud, $\gamma_{EXD,TE} = Span_{norm} * \gamma_{EXD,TE,SHR}$, being $\gamma_{EXD,TE,SHR}$ the design variable to be varied during optimization.

In sum, for the generation of a new tandem design:

1. Inverse design solver computes exducer 3D geometry:
    a. $\gamma_{EXD,TE,SHR}$ and $rV^*_{\theta}{}_{ratio}$ are inputs;
    b. $\gamma_{EXD,LE}$ is obtained;
2. Inverse design solver computes inducer 3D geometry:
    a. $\gamma_{IND,TE}$ is an input (computed for an input $\Delta\lambda_{SHR}$).

RADIVER COMPRESSOR

The measurements on the test case "RadiVer" were carried out at the Institute of Jet Propulsion and Turbomachinery at RWTH Aachen University, Germany. Part of the investigations was funded by the Deutsche Forschungsgemeinschaft (DFG). The data was presented by Ziegler et al. in two studies, initially in an experimental study of the interaction between impeller and wedge diffuser [20], and in a detailed flow analysis study [21]. From then on, the Radiver compressor geometry and test data have been used as a test case for various studies. The same compressor is used in this study to validate the numerical setup used during design iterations. The main goal of the present study is to conclude regarding the advantages or shortcomings of tandem-blade impeller design, so the vaneless diffuser case of the Radiver compressor is used. Relevant geometrical information of the Radiver compressor is summarized in Table 1.

The design rotation speed is of 35200 rpm. A mesh sensitivity study is carried out at 80% design speed and at a corrected mass flow rate of 1.98 $kg\ s^{-1}$. With the final chosen mesh value, comparison of performance curve is then made against test data for 3 speed lines (60%, 80% and 100%). Impeller redesign is then performed at 100% of the design speed and at corrected mass flow of 2.405 $kg\ s^{-1}$. Impeller transonic flow is found at design point, with inlet tip relative Mach number of 0.945. The stall and choke margin at 100% rotation speed are determined by CFD analysis at 2.272 $kg\ s^{-1}$ and at 2.533 $kg\ s^{-1}$, respectively.

ANSYS CFX (2020R2) was used for the CFD analysis in this study. The turbulence model was k-omega SST with high resolution advection scheme. Single-phase, steady state analysis was performed, using air as ideal gas as the working fluid. Total pressure and total temperature are imposed at the inlet as boundary conditions, and mass flow is specified at the outlet. A single-passage model was assembled, with application of rotational periodic boundary conditions. The computational domain used is presented in Figure 3. Frozen rotor interfaces were applied between inlet and impeller domain, and between impeller and vaneless diffuser domain. No-slip wall boundary conditions are specified for all walls except for the inlet domain hub wall, which is defined as a free slip wall.

Table 1 - Radiver geometry data

Number of blades	15
Impeller diameter	270 mm
Impeller Outlet width	11 mm
Diffuser outlet diameter	690 mm
Inlet shroud diameter	145.8 mm
Axial length	83.96 mm
Tip clearance	0.7 mm

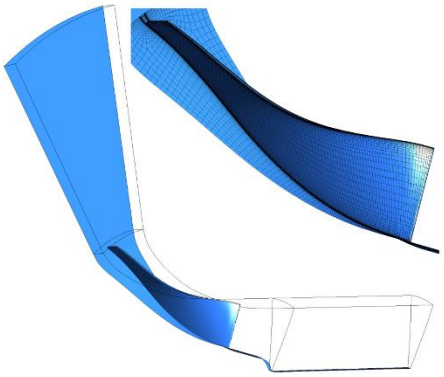

Figure 3 - Radiver computational domain

A mesh sensitivity study was carried out on performance and entropy generation parameters, with four mesh levels of increased refinement being tested. Table 2 shows the mesh element count and CFD parameters for the different levels. Average Y+ on the blade surface is kept under 5 for all designs, and under 1 for the Fine and Very fine levels.

Table 2 - Mesh sensitivity study for Radiver compressor

	Elements (Million)	Y+ average on blade surface (-)	$\dot{S}$ (W/K)	η_{IMP} (-)	PR_{IMP} (-)
Coarse	1.25	2.36	2.65	91.22	2.61
Medium	2.5	2.17	2.76	91.63	2.618
Fine	5.6	0.94	2.86	91.86	2.621
Very fine	10.11	0.87	2.89	92.01	2.632

The data in Figure 4 is normalized against the values obtained for the very fine mesh size. For entropy generation rate, coarse and medium mesh levels present a deviation of more than 5% for the impeller domain against the reference value, whereas the fine mesh shows a deviation of approximately 2% against the reference. For pressure ratio, for all mesh sizes, stage and impeller pressure ratios are inside a 1% margin against the reference. The fine mesh is used for entropy analysis, whereas medium mesh level is used during design iterations, as it is seen to be sufficient for the accurate prediction of the performance parameters of relevance during the design stage.

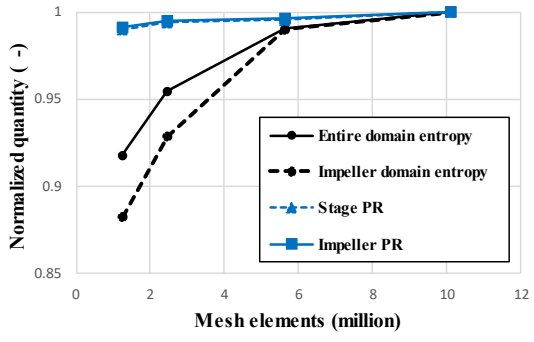

Figure 4 - Entropy generation rate (black) and pressure ratio (blue) against mesh size (black)

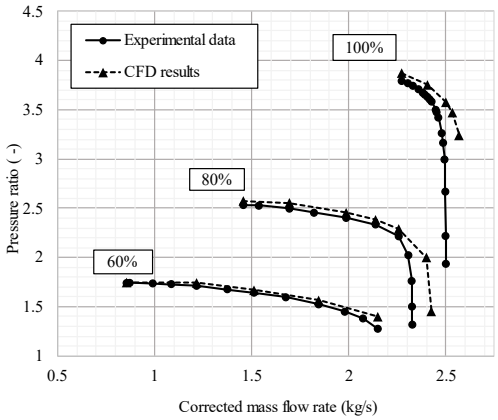

Figure 5 - Radiver compressor map

Using the described CFD model and mesh level, the Radiver compressor map is generated for 3 different speed lines, presented in Figure 5. A good agreement is seen between CFD and experimental data. As backplate leakage is not included in the model, a shift of CFD results to higher flow rates is not unexpected and the choke margin is overpredicted in CFD by around 2.7% (at 100% speed). At

the design point, a pressure ratio of 3.751 is obtained numerically, comparing against a pressure ratio of 3.630 obtained in test, representing a 3.3% difference.

ANSYS Mechanical (2020R2) is then used for structural FE analysis. Titanium was used as material, with Young modulus of 115 GPa, density of 4429 $kg\ m^{-3}$and Poisson ratio of 0.34. The backplate geometry was generated in CAD from Radiver technical drawings and a fillet of constant 2.5 mm radius was generated. Cylindrical supports have been defined at the bottom portion of the backplate – where connection with rotation vane exists - and a fixed support at the back portion. Rotational speed of 35200 rpm was imposed. Figure 6 presents the equivalent (Von mises) stress distribution throughout the blade, fillet and hub surfaces. The maximum stress identified is of 340.46 MPa and is located at the hub, suction side, trailing edge area.

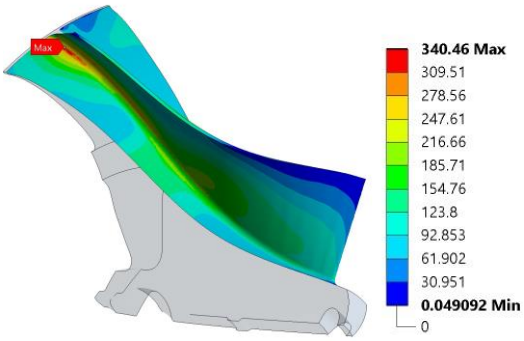

Figure 6 - Radiver equivalent stress distribution at rot. speed = 35200 rpm; Max = 340.46 MPa

From the presented analysis of the Radiver compressor, the design requirements to be obtained numerically for the tandem blade designs can be summarized. At the design point, a minimum pressure ratio of 3.75 should be obtained, with stage efficiency higher than 81.05%. Also, similar stall and choke margin should be obtained - by meeting pressure ratio and efficiency at low and high mass flow operating points without fluctuations in CFD - and, ideally, a maximum equivalent stress in blade region of around 340 MPa.

BASELINE TANDEM-BLADE DESIGN

A baseline design that meets the basic requirements obtained from the Radiver test case analysis has been generated with the 3D inverse design method to serve as a starting point for the optimization procedure. The required inputs for the baseline tandem design are summarized and addressed: meridional channel geometry; thickness distribution; blade loading distribution; and stacking distribution at the exducer trailing edge.

The meridional channel has hub and shroud curves same as the Radiver compressor. The inducer leading edge (LE) and exducer trailing edge (TE) are also matched with the Radiver geometry. Exducer LE is placed at 27.17% and 24.90% of the meridional distance of the full blade, at hub and shroud, respectively. The exducer LE meridional location is chosen as performed in previous tandem-blade design studies, such as done by Li et al. [14], where the LE is placed in the location where the meridional path starts the turning from axial to radial direction. Some amount of overlapping is considered necessary to avoid interaction between the inducer's wake and the exducer LE, and so, this parameter is taken as a small percentage of the meridional extent (1.08% at hub and 1.78% at shroud), resulting in an inducer trailing edge positioning of 28.26% and 26.68% of the meridional distance, respectively at hub and shroud. Figure 7 shows the meridional channel of baseline design.

The thickness distribution was adjusted to keep the maximum equivalent stress under the threshold found for the Radiver compressor. Initially, a design with reduced thickness at shroud and similar thickness at hub, for both blades, was tested. The high structural stresses obtained required the thickness at the hub of the exducer blade to be increased, as illustrated in Figure 8.

The blade angle distribution is not same as Radiver compressor, as it is obtained as an output of the inverse design solver. The solver requires the specification of $r\overline{V_\theta^*}$ values at LE and TE, and streamwise blade loading distribution ($\partial r\overline{V_\theta^*}/\partial m$) from LE to TE.

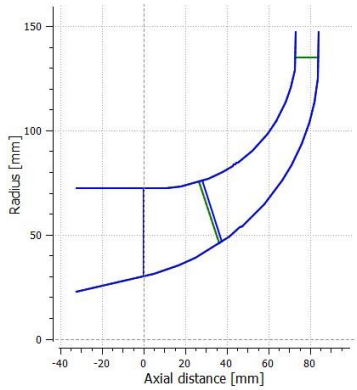

Figure 7 - Meridional channel for baseline design.

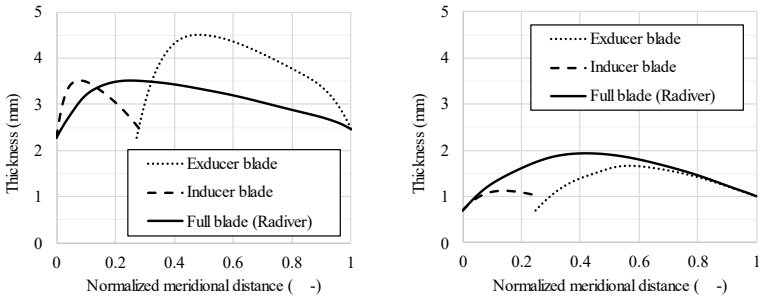

Figure 8 – Hub (left) and shroud (right) thickness distribution for baseline design against Radiver design

The spanwise $r\overline{V_\theta^*}$ split between both blades is an important design parameter and is varied during the design procedure. For the baseline design, $r\overline{V_\theta^*}_{ratio} = 0.1$, which means 10% of the work is being performed by inducer, and 90% by exducer. For the inducer, $r\overline{V_\theta^*}_{LE} = 0$, as no inlet swirl exists, and $r\overline{V_\theta^*}_{TE} = 0.0705$, accounting for 10% of the overall $r\overline{V_\theta^*}$. For exducer, $r\overline{V_\theta^*}_{LE} = 0.0705$, matching the TE value for inducer, and $r\overline{V_\theta^*}_{TE} = 0.705$, ensuring the baseline design has the same pressure ratio as the Radiver compressor at the design point.

The streamwise blade loading ($\partial r\overline{V_\theta^*}/\partial m$) is presented in Figure 9 for both blades. This parameter is used to shape the 3D blade geometry and directly relates to the pressure jump across the blade. For the baseline case, the blade loading distribution was adjusted taking into account previous knowledge regarding centrifugal compressor design using inverse design [17]. $\partial r\overline{V_\theta^*}/\partial m$ at the LE (streamwise location = 0) controls the incidence and throat area of the design. For the inducer, this value was adjusted to obtain similar stall and choke margins as the Radiver case. Regarding the exducer, $\partial r\overline{V_\theta^*}/\partial m$ at LE was adjusted from hub to shroud in order to obtain small LE lean and bow, keeping structural stress at a reasonable level for the exducer blade.

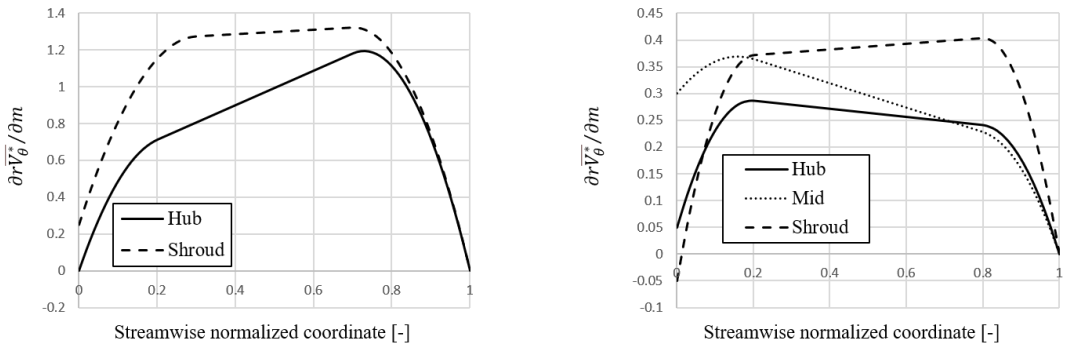

Figure 9 - Blade loading distribution for exducer (left) and inducer (right)

Regarding trailing edge wrap angle, for the baseline design, $\gamma_{EXD,TE,SHR} = 0$, resulting in a constant wrap angle spanwise distribution for the exducer blade at the trailing edge. Regarding the inducer, the wrap angle distribution at the trailing edge is determined by the circumferential clocking distribution λ, which is determined by $\Delta\lambda_{SHR} = 0$. Figure 2 presents the full spanwise clocking distribution for the baseline design.

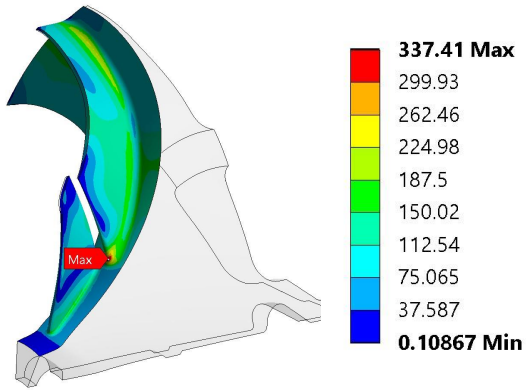

Figure 10 - Tandem baseline design equivalent stress distribution; Max = 337 MPa

The structural FEA has shown a shift in highest stress location to the exducer LE hub region, as seen in Figure 10, having a maximum of 337 MPa, just under the requirement set from the Radiver test case analysis. The fillet radius has been adjusted to 3mm for exducer blade (27.2% of the exducer outlet width) and to 1mm for inducer blade (9.07% of the inducer hub meridional length). From CFD, the pressure ratio for baseline tandem design is met at the 4 operating points and the stage total-total efficiency is slightly reduced at design point and only increased at high flow rate.

OPTIMIZATION

Optimization of the baseline design was performed with the objective of increasing efficiency at the design point. The optimization approach lies in performing a Design of Experiments (DoE) and generating a response surface model using the data collected, on top of which the optimization is performed. Candidate points are then chosen and evaluated in CFD and FEA. The optimization formulation is detailed:

1. The input parameters and specified ranges are detailed in Table 3 (λ_{SHR} is a function of $\Delta\lambda_{SHR}$).
2. The optimization objectives are set to minimize the diffuser loss coefficient, defined as $(P_{OUT} - P_{IN})/P_{DYN,IN}$, and maximize the impeller efficiency. It should be clarified that maximizing impeller efficiency and minimizing diffuser losses ultimately results in increased stage efficiency.
3. The constraint of keeping pressure ratio above 3.8 is set.

Table 3 - Input ranges for design of experiments

Input	Baseline	DOE lower limit	DOE upper limit	Optimized
$rV^*_{\theta\,ratio}$	0.1	0.08	0.18	0.139
$\Delta\lambda_{SHR}$	0%	-6%	13.5%	-7.06%
λ_{SHR}	23.77%	17.77%	37.27%	16.71%
$\gamma_{EXD,TE,SHR}$	0	-4	2.0	0.283

A design of experiments with 32 candidates was carried out, with Latin Hypercube sampling being used to generate the design space. During the DOE, strong correlations between impeller efficiency and $rV^*_{\theta\,ratio}$ and between diffuser loss coefficient and exducer stacking angle were observed. An optimal $rV^*_{\theta\,ratio}$ value appears evident at around 0.14 from examining the left chart of Figure 11. Low correlation between circumferential clocking and performance parameters is seen. A Kriging response surface is assembled in ANSYS Workbench 2020R2 and optimization is performed using Multi-Objective Genetic Algorithm (MOGA).

The optimized design parameters are presented in Table 3 and can be compared against the baseline input values. $rV^*_{\theta\,ratio}$ is increased, shifting some of the workload on to the inducer blade, negative $\Delta\lambda_{SHR}$ represents the inducer-exducer gap at the shroud being reduced and a slight positive $\gamma_{EXD,TE,SHR}$ representing the exducer shroud, at the TE, leaning in the rotational direction.

Figure 12 shows the values for diffuser loss coefficient versus impeller efficiency: on the left, the DOE data evaluated in CFD shows some designs with improved impeller efficiency, and no design

with considerable better diffuser loss coefficient; middle and right charts show the evaluations performed on the Kriging response surface, the pareto front and optimized design chosen.

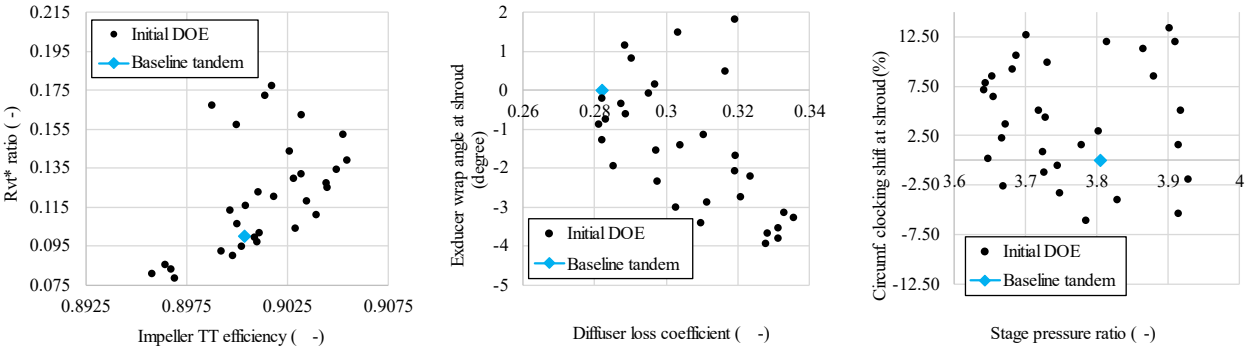

Figure 11 -Data collected from DOE procedure: left: $r\overline{V^*_{\theta_{ratio}}}$ against impeller efficiency; Middle: $\gamma_{EXD,TE,SHR}$ against diffuser loss coefficient; Right: $\Delta\lambda_{SHR}$ against stage pressure ratio.

Figure 13 shows the equivalent stress distribution of the optimized design. It is seen that the stress distribution has changed in relation to the baseline tandem design, and the highest stresses have now shifted to the inducer LE, close to the hub location. This change in location of the maximum stresses required the fillet radius to be increased to 3mm for inducer blade (27.2% of the exducer outlet width), in order to keep structural stress to a minimum for this design. The exducer fillet radius was reduced to 1mm (9.07% of the exducer outlet width), in order for both fillets to fit in the gap between blades.

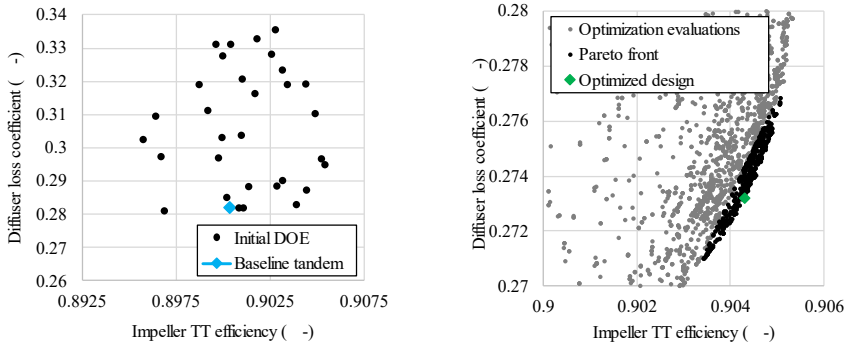

Figure 12 - Diffuser loss coefficient versus impeller efficiency - Left: DOE data obtained from CFD; Middle: Right Optimization evaluations, including pareto front, using Kriging response surface;

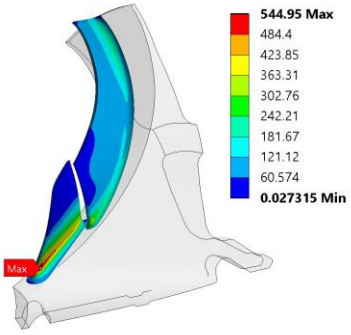

Figure 13 - Tandem optimized design equivalent stress distribution; Max = 544 MPa

Being the tensile strength of Titanium varying around 700MPa and 860MPa for the range of operating temperatures of the compressor, the maximum stresses are still under this limit, by a margin of around 20-40%. It was verified that the LE lean angle has increased during the design optimization, and constraining this parameter during optimization can help keep structural stresses contained. Besides this, the inducer thickness at hub was not increased in relation to Radiver design and an adjustment to this can also improve the structural performance of the baseline design without major compromise to aerodynamic performance.

Table 4 presents the flow and work coefficients, and efficiency for the 3 designs studied, in order to illustrate the change in global performance. The work coefficient was increased from Radiver to the Optimized tandem designs, while flow coefficient is reduced.

Table 4 – Performance parameters

	Radiver	Baseline tandem design	Optimized tandem design
Flow coefficient	0.059	0.059	0.059
Work coefficient	0.6805	0.6902	0.6981
Efficiency	81.05%	80.95%	81.5%

A geometry comparison is performed between baseline and optimized designs. Figure 14 shows a comparison of blade angle distribution between the baseline and optimized tandem blade designs. The increased loading of inducer blade for the optimized design, as a result of the optimization procedure, is evident from the decreased TE blade angle of the inducer.

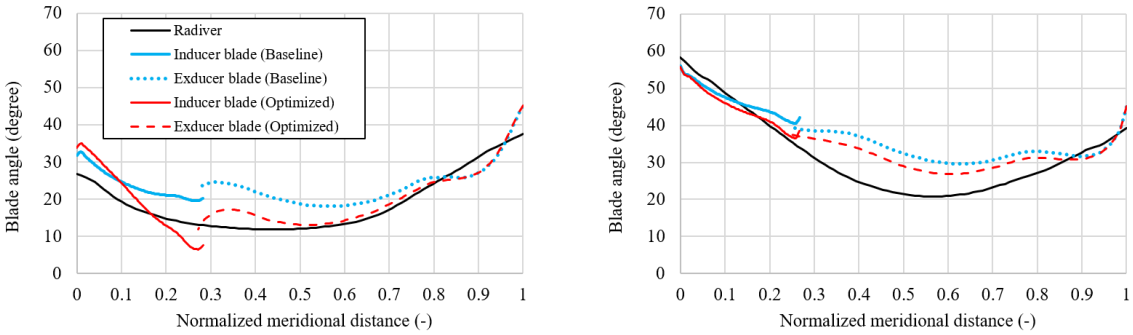

Figure 14 - Blade angle distribution comparison between Radiver, baseline and optimized tandem designs; Left: Hub; Right:Shroud

Figure 15 shows the performance maps of baseline and optimized designs. The efficiency was measured at the vaneless diffuser outlet. A 0.5% efficiency improvement is seen at design point. The stall choke margins stay similar to the previous designs and an increase in pressure ratio is observed at all design points for the optimized design.

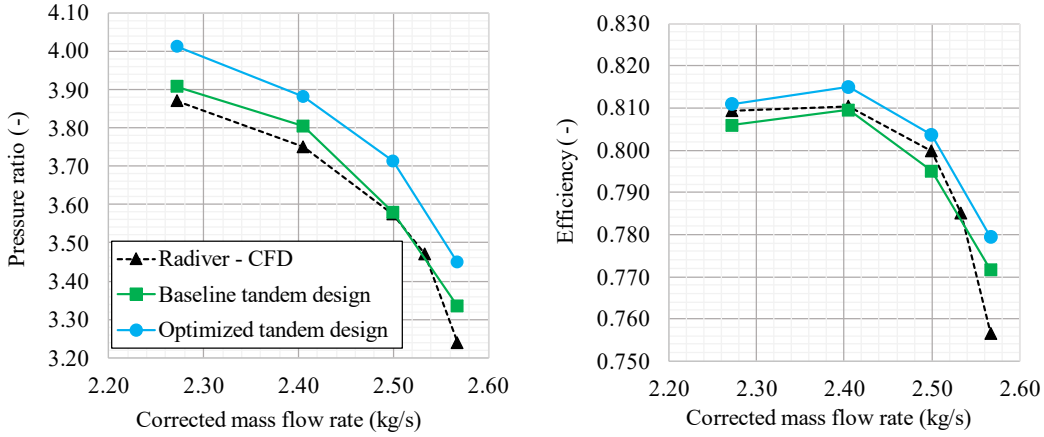

Figure 15 - Performance curves for Radiver test case, baseline and optimized tandem designs.

An entropy analysis is subsequently performed on the Radiver test case, baseline tandem design and optimized tandem design to better understand the flow physics and the mechanism of performance improvement. The methodology presented in [18] is followed, decomposing the impeller flow domain in different zones by using different loss mechanisms as criteria. Four zones are captured, relating to shock, tip leakage, boundary layer and secondary flow losses. These were shown to capture the main losses in the impeller passage.

Figure 16 presents, at the design point, the entropy generation rate for the different zones identified for the 3 designs studied. It is seen that for all designs, of the 4 loss zones discriminated, tip vortex and boundary layer represent the major loss contributors. Shock losses and secondary flow represent a minor contribution to the overall losses, and there is a slight increase in these quantities from the Radiver to the tandem designs.

Tip vortex losses are reduced from the full blade Radiver design to both the baseline and optimized tandem designs and can be seen as the main contributor to the efficiency improvement seen in the optimized tandem design.

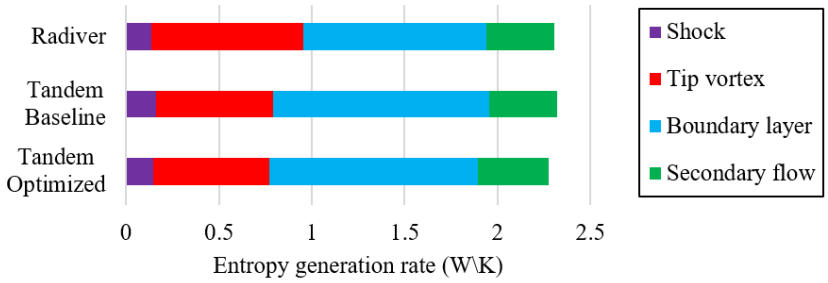

Figure 16 - Entropy generation rate for different zones, for Radiver, baseline tandem and optimized design.

Figure 17 show the tip leakage streamlines for the initial Radiver full blade design and the tandem blade optimized design. Also, contours of static entropy are plotted at constant streamwise locations close to the trailing edge. It is clear that the static entropy contours show reduced high entropy area, especially closer to the trailing edge. This is consistent with the loss analysis shown in Figure 14. The tip leakage loss is reduced in the tandem blade designs, compared to the full blade design.

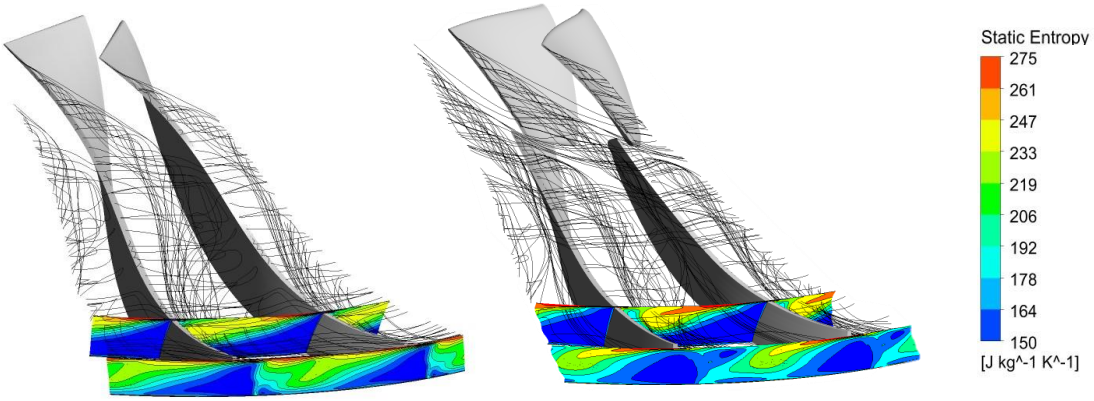

Figure 17 - Tip leakage loss generation zone; left: Radiver compressor; right: Optimized tandem design

Boundary layer losses increase with tandem blade configurations, which can, in part, be explained by the larger blade surface on the tandem designs. The surface area increases by 8.0% from initial full blade Radiver to the baseline tandem design. After the optimization, the optimized design shows 7.3% increased blade surface area against Radiver compressor. The surface area change is visible in the geometry comparison in Figure 18.

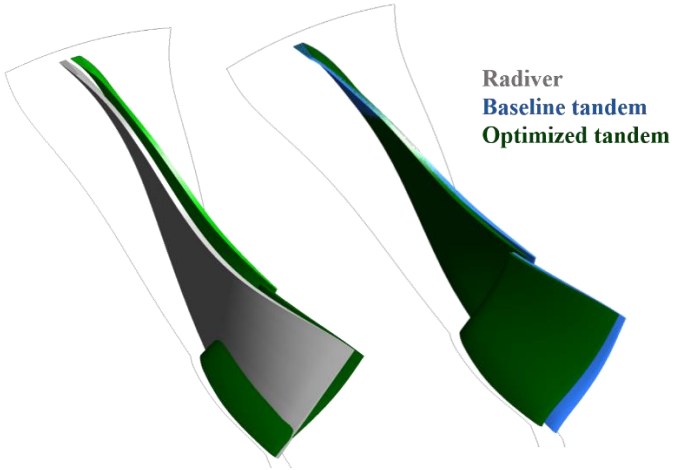

Figure 18 - 3D geometry comparison between Radiver and Optimized tandem design (left); and between Optimized and baseline tandem designs (right)

In the boundary layer flow zone, it was also seen that some part of the inducer wake is included in this region. The inducer wake is an extra source of loss, present in the tandem blade arrangement, and also contributes to the higher losses in the boundary layer flow region. Besides this, also the jet effect produced between inducer and exducer, although beneficial in restarting the boundary layer, generates higher velocities on the exducer suction side, contributing to the higher losses.

In Figure 19 the static entropy contour at 30% spanwise position is presented. The tip vortex region is evident close to the trailing edge suction side, where a more intense and extense entropy generation area is seen for the full blade design, supporting the conclusion that tip vortex losses are reduced with the tandem arrangement. The entropy generation due to the inducer wake is also visible in Figure 19. Finally, the boundary layer losses are also evident, as boundary layer growth, although interrupted by the inducer/exducer gap, restarts and rapidly grows in the exducer blade.

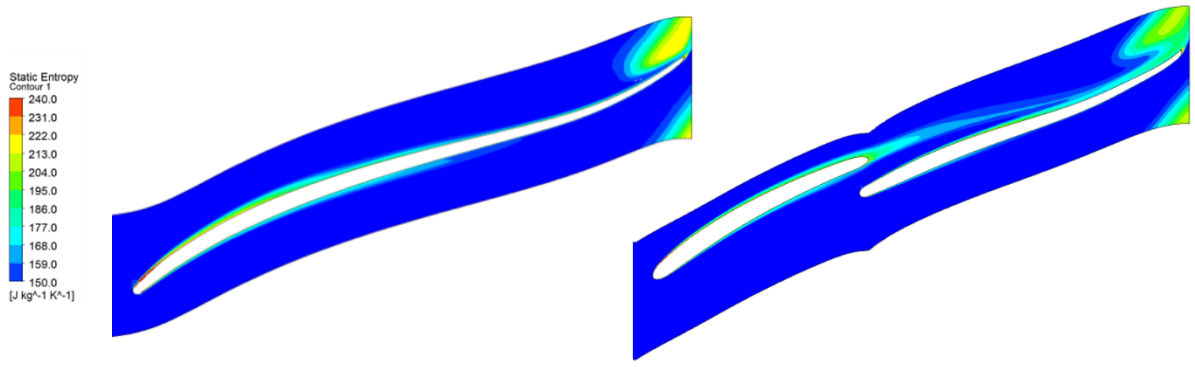

Figure 19 - Blade to blade velocity contour at 50% spanwise position. Comparison between Radiver (left) and optimized tandem design (right).

Regarding the optimization procedure, it was seen that an optimal $rV^*_{\theta_{ratio}}$ value exists (refer to Figure 11, left chart). Attributing a low amount of loading to the inducer blades results in higher surface area and profile losses, resulting in lower impeller efficiency. On the other hand, increasing $rV^*_{\theta_{ratio}}$, in this way attributing higher amount of loading to the inducer blade, can possibly result in over loading the inducer, leading to separation or incidence issues on the exducer blade.

The optimization proved to be essential in finding the optimal value of $rV^*_{\theta_{ratio}}$ to obtain higher efficiency. The boundary layer losses are reduced from baseline to optimized design, as can be seen in Figure 16. Comparing the optimized and baseline tandem designs, the reduced surface area, caused by shifting the loading to inducer blade, resulted in lower boundary layer loss and higher efficiency of the optimized design.

CONCLUSIONS

In this work, a specifically assembled methodology, based on the 3D inverse design of exducer and inducer blades is presented. The method was applied to the optimization of the Radiver compressor and improved performance was obtained. Structural analysis was performed through FEA, and loss analysis was carried out on the designs obtained (through an entropy generation quantification based on the flow domain decomposition by loss generation mechanism). With this study, a few conclusions are drawn: Firstly, the tandem blade configuration improved the radial compressor performance by reducing tip leakage vortex loss. Boundary layer losses increased in the tandem blade configurations, due to higher surface area, inducer wake, and due to higher exducer surface velocity. The increase in boundary layer loss can counteract the improvement obtained by tip vortex loss reduction. An optimization-based approach can be adopted to reduce boundary layer loss in order to achieve an improved design. The tandem blade optimized design did not compromise the

off-design performance, and the stall and choke margins are maintained. Improved efficiency and increased pressure ratio at all operating points in the studied speed line is seen.

Secondly, to take the advantage of the tandem blade design, a balance between different losses is needed. The inverse design-based optimization approach can effectively explore the design space and generate good quality candidates. The design methodology assembled can easily control the loading distribution between inducer and exducer, which is seen to be a crucial parameter when design compressors with a tandem blade configuration. The coupling between the inducer and exducer can be included in the design approach, which eases the effort on design iterations based on blade angle parameterization and CFD feedback.

Bibliography

[1] H. Klassen, J. Wood and L. Schumann, "Experimental Performance of a 13.65-Centimeter-Tip-Diameter Tandem-Bladed Sweptback Centrifugal Compressor Designed for a Pressure Ratio of 6," NASA, Cleaveland, Ohio, 1977.

[2] G. Bache, "Impeller tandem blade study with grid embedding for local grid refinement," in *Tenth Workshop for Computational Fluid Dynamics Applications in Rocket Propulsion*, Huntsville, Alabama, 1992.

[3] D. A. Roberts and S. C. Kacker, "Numerical Investigation of Tandem-Impeller Designs for a Gas Turbine Compressor," in *ASME TURBO EXPO*, New Orleans, Louisiana, 2001.

[4] Y. P. Ju and C. H. Zhang, "Design Optimization and Experimental Study of Tandem Impeller for Centrifugal Compressor," vol. 30, no. 6, 2014.

[5] B. Josuhn-Kadner and B. Hoffmann, "Investigations on a Radial Compressor Tandem-Rotor Stage with Adjustable Geometry," in *International Gas Turbine and Aeroengine Congress and Exposition*, Cologne, 1992.

[6] B. Josuhn-Kadner, "Flow Field and Performance of a Centrifugal Compressor Rotor with Tandem Blades of Adjustable Geometry," in *International Gas Turbine and Aeroengine Congress and Exposition*, The Hague, 1994.

[7] S. Danish, S. Qureshi, A. El-Leathy, S. Ud-Din, U. Umer and M. Chaochen, "Numerical Investigation & Comparison of a Tandem-Bladed Turbocharger Centrifugal Compressor Stage with Conventional Design," *Journal of Thermal Science*, 2014a.

[8] R. R. Erdmenger and V. Michelassi, "Influence of Tandem Inducers on the Performance of High Pressure Ratio Centrifugal Compressors," in *ASME Turbo Expo*, Montreal, 2015.

[9] X. Shi, J. Lu and L. Zhao, "Investigations on the influence of tandem blades on inner flow and performance characteristics of centrifugal pump," vol. 234, 2019.

[10] Z. Li, G. Han, X. Lu, E. Huang and S. Zhao, "Improving the operating range using a centrifugal compressor with a tandem impeller," 2019a.

[11] Z. Li, S. Zhao, X. Lu, G. Han, C. Yang and J. Zhu, "Inducer/Exducer Matching Characteristics inside Tandem Impellers of a Highly Loaded Centrifugal Compressor," 2020.

[12] N. Cuturi and E. Sciubba, "Design of a Tandem Comressor for the Electrically-Driven Turbocharger of a Hybrid City Car," *Energies*, 2021.

[13] S. N. Danish, S. U.-D. Khan, U. Umer, S. R. Qureshi and C. Ma, "Performance Evaluation of Tandem Bladed Centrifugal Compressor," vol. 8, no. 3, 2014b.

[14] Z. Li, X. Lu, S. ZHAO, G. Han, C. Yang and Y. Zhang, "Numerical investigation of flow mechanisms of tandem impeller inside a centrifugal compressor," *Chinese Journal of Aeronautics,* p. 13, 2019b.

[15] L. Advanced Design Technology, *TURBOdesign Suite, Version 2021,* London, 2021.

[16] M. Zangeneh, "A Compressible Three Dimensional Blade Design Method for Radial and Mixed Flow Turbomachinery Blades," *Int. J. Numer Methods Fluids,* pp. 599-624, 1991.

[17] M. Zangeneh, "On 3D Inverse Design of Centrifugal Compressor Impellers With Splitter Blades," *ASME 1998 International Gas Turbine and Aeroengine Congress and Exhibition,* pp. 98-GT-507, 1998.

[18] L. Zhang, L. Kritioti, P. Wang, J. Zhang and M. Zangeneh, "A Detailed Loss Analysis Methodology for Centrifugal Compressors," *Journal of Turbomachinery,* 2022.

[19] L. Zhang, S. R. Ray and M. Zangeneh, "Application of 3D Inverse Design Method on a Transonic Compressor Stage," in *Turbomachinery Technical Conference and Exposition*, Rotterdam, 2022.

[20] K. Ziegler, H. E. Gallus and R. Niehuis, "A Study on Impeller-Diffuser Interaction - Part I: Influence on the Performance," *Journal of Turbomachinery,* pp. 173-182, 2002a.

[21] K. U. Ziegler, H. E. Gallus and R. Niehuis, "A Study on Impeller-Diffuser Interaction: Part II - Detailed Flow Analysis," 2002b.

[22] "Performance Evaluation of Tandem Bladed Centrifugal Compressor," 2014.

